VNU Journal of Science: Mathematics - Physics

Journal homepage: https://js.vnu.edu.vn/MaP

Original Article

Photoluminescent Properties of Red-emitting $AlPO_4:Cr^{3+}$ Phosphor for Plant Growth LEDs

Tran Manh Trung[1], Nguyen Tu[1,*], Nguyen Van Quang[5], Do Quang Trung[1], Pham Thanh Huy[1,2]

[1]*Phenikaa University, Yen Nghia, Ha Dong, Hanoi, Vietnam*

[2]*Phenikaa Research and Technology Institute (PRATI), Phenikaa University, A&A Green Phoenix Group, 167 Hoang Ngan, Hanoi, Vietnam*

[3]*Hanoi Pedagogical University 2, Xuan Hoa, Vinh Phuc, Vietnam*

Received 16 October 2020
Revised 23 November 2020; Accepted 01 December 2020

Abstract: In this study, red-emitting $AlPO_4:Cr^{3+}$ phosphors have been successfully synthesized by a facile sol-gel method. The Tanabe–Sugano diagram demonstrates that the surrounding sites of Cr3+ ions have a high crystal field with Dq/B=2.47. The sharp 694-nm peak on the PL of $AlPO_4:Cr^{3+}$ phosphor could be attributed to the $^2E \rightarrow {}^4A_2$ electron transition of Cr^{3+} ions. The $AlPO_4$:0.3%Cr^{3+} phosphor presents the highest PL intensity, then a purple LED prototype is obtained by coating the optimum powder on a UV LED chip. The color coordinates (0.2412, 0.1330) of the purple LED prototype imply that $AlPO_4:Cr^{3+}$ phosphors are promosing to be used as deep red phosphor powder for horticulture LED lighting.

Keywords: Phosphor material, $AlPO_4:Cr^{3+}$, sol – gel method, horticulture lighting, plant growth LED.

1. Introduction

With the rapid growth of world economy and population, the energy and environment are the two emerging issues attracting an increase in attention [1]. Besides the accelerated growth of light-emitting diodes (LEDs) lighting, it is highly demanded to innovate commercial artificial greenhouse planting technology in order to obtain high-standard vegetables and green grains [2–5]. Comparing to the conventional light sources (e.g., fluorescent lamp, incandescent lamp, and metal halide lamp etc.), LED

*Corresponding author.
Email address: tu.nguyen@phenikaa-uni.edu.vn

https//doi.org/ 10.25073/2588-1124/vnumap.4617

has been considered as a new interesting light source because of many advantages such as low energy consumption, low radiant heat output, high performance, eco-friendliness, and long lasting [6]. It is well known that the blue (430–520 nm), red to deep-red (630–750 nm) light are crucial for the growth of plants because they are responsible for photosynthesis, phototropism, and photomorphogenesis, respectively [7]. Importantly, it is possible to adjust the spectral composition of LED based on the absorption spectrum needed for plants growth by designating suitable phosphors which are often blue and red phosphors [8]. Therefore, the high demand for deep-red-emitting phosphors has been recently received a great attention [2]. Theoretically, red light could be generated by converting a part of violet emission from a violet LED chip using suitable phosphors powder [6]. Up to now, rare-earth ions such as Eu^{3+}, Sm^{3+}, Ce^{3+} have been mostly used for commercial red-emitting phosphors because of their high luminescent efficiency [6, 8–16]. However, they still have several major drawbacks includinghigh price , high undesirability near-UV absorption, environmentally unfriendliness and insignificant far-red light, which limit their applications in horticulture lighting [2, 3]. In contrast, the transition-metal-based phosphors exhibit many superior properties like non-toxicity, low cost and ablity to emit far-red emission. Hence, it is very promising to use them instead of rare earth-based materials [3, 8, 14]. Unfortunately, their biggest disadvantage is the low luminescent efficiency.

In the group of transition metal ions, Cr^{3+} ion with the unfilled ($3d^3$) electrons is a promising candidate for far-red growth LED because the Cr^{3+}-based phosphors have not only two strong absorption bands peaking around ~410 and ~560 nm but also remarkable red/far-red emissions [3,6,14–16,18]. In addition, it is worthy to note that crystal fields have a strong influence on the emission spectra of Cr^{3+} ions [19,20]. Hence, this issue is a major challenge for the scientists and researchers. Owning fantastic properties such ashigh availability , low cost , superior chemical resistance and thermal steadiness, $AlPO_4$ matrix is prevalently used as an artificial frame over a large range of temperature from 400 to 800 °C [21]. According to the literature, the synthesis of Cr^{3+}-doped $AlPO_4$ phosphor and the effect of crystal field on its optical properties; however, have not been studied yet.

Herein, the far-red-emitting $AlPO_4:Cr^{3+}$ phosphor has been successfully synthesized by a simple sol-gel method. The influence of annealing temperature and Cr^{3+} level on the phase structure, morphology, and optical properties have been thoroughly investigated. The correlation between the luminescent properties of $AlPO_4:Cr^{3+}$ phosphor and crystal field has also been studied. A proof of coated-phosphor LED concept has also been fabricated to demonstrate the performance of red emission.

2. Experimental

$AlPO_4:Cr^{3+}$ powder was fabricated by a simple sol-gel method using these starting materials: aluminum nitrate nonahydrate ($Al(NO_3)_3.9H_2O$, 99.9%), chromium (III) nitrate nonahydrate ($Cr(NO_3)_3.9H_2O$, 99.9%), citric acid ($C_6H_8O_7$, 99.5%) and ammonium dihydrogen phosphate ($NH_4H_2PO_4$, 99.9%). Firstly, $Al(NO_3)_3.9H_2O$, $Cr(NO_3)_3.9H_2O$ and citric acid with the calculated weight ratio, as shown in Table 1, were dispersed in deionized water using a magnetic stirrer at ambient. Then, 9.2 g $NH_4H_2PO_4$ was presented, then the obtained product was magnetically stirred at 120 °C to completely remove the residual water prior to achieving a high-viscosity crystal-clear gel. The obtained product was further dehydrated at 150 °C for 3 − 5 h to get a moitureless gel. In the last step, the dry gel was annealed at various temperatures in the range of 1200 − 1500 °C for 5h in air to get $AlPO_4:Cr^{3+}$ powder.

The morphology structure was characterized by a field emission scanning electron microscopy (SEM – Hitachi S4800). The XRD pattern of $AlPO_4:Cr^{3+}$ powder was determined by an X-ray

diffractometer (D8 Advance, Bruker) equipping with a CuKα radiation source (λ_{Cu}=1.5406 Å); in which, the 2θ is scanned from 15 to 65° with a step of 0.02°. The excitation and emission spectra were carried out at ambient by a NanoLog fluorescence spectrophotometer (Horiba) equipped with a 450 W xenon discharge lamp as the excitation source.

Table 1. The different amounts of raw materials for synthesize $AlPO_4:xCr^{3+}$ phosphors

Sample	$Al(NO_3)_3.9H_2O$ (g)	$NH_4H_2PO_4$ (g)	$Cr(NO_3)_3.9H_2O$ (g)	Citric acid (g)
$AlPO_4:0.1\%Cr^{3+}$	29.97	9.2	0.032	16.8
$AlPO_4:0.3\%Cr^{3+}$	29.91	9.2	0.096	16.8
$AlPO_4:0.5\%Cr^{3+}$	29.85	9.2	0.16	16.8
$AlPO_4:0.7\%Cr^{3+}$	29.79	9.2	0.224	16.8
$AlPO_4:1\%Cr^{3+}$	29.7	9.2	0.32	16.8
$AlPO_4:1.5\%Cr^{3+}$	29.55	9.2	0.48	16.8

3. Results and Discussion

Figures 1a&b show the FESEM image and XRD pattern of $AlPO_4:0.3\%Cr^{3+}$ phosphor thermally treated at 1500 °C for 5h in air, respectively. It is noticed that the particle size is varying from submicrometers to several micrometers. As shown in Figure 1b, both two crystalline phases $AlPO_4$ (JCPDS 11-0500) [22] and CrO_3 (JCPDS 32-0285) [21] are co-existed in the XRD of the obtained sample. In which, the peaks at 2θ = 21.9°; 25.55°; 28.30°; 31.24°, and 36.03° respectively correspond to (111), (020), (021), (112) and (220) planes of the orthorhombic $AlPO_4$ structure (JCPDS 11-0500) [21, 22].

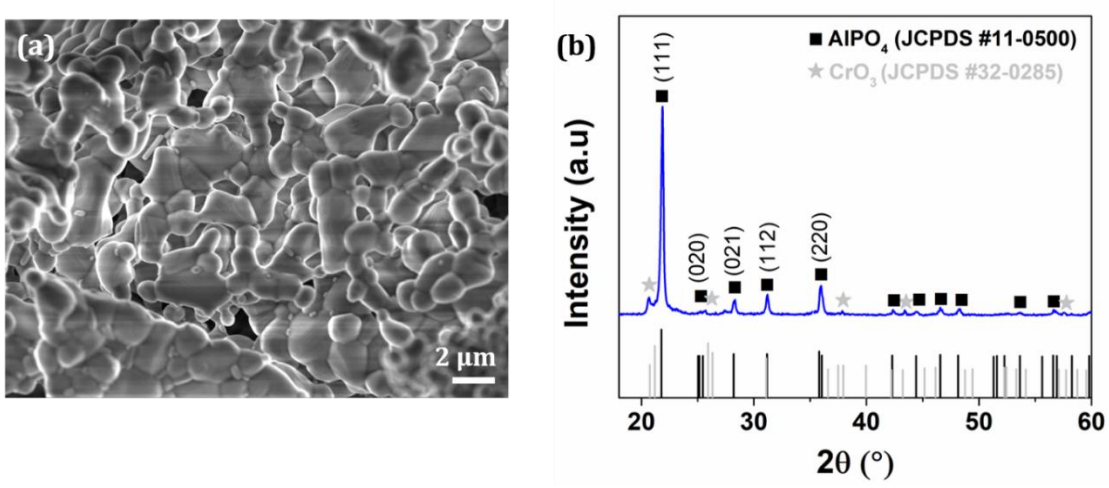

Figure 1. (a) FESEM image and (b) XRD pattern of $AlPO_4:0.3\%Cr^{3+}$ phosphor air-annealed at 1500 °C for 5h.

Figure 2 illustrates PLE and PL spectra of the $AlPO_4:0.3\%Cr^{3+}$ phosphor air-annealed at 1500 °C for 5h (λ_{ex} = 395 nm). The PLE spectrum in Figure 2a indicates that the materials absorb intensely with two bands peaking at about 396 and 556 nm. These absorptions are assigned to spin-allowed $^4A_2 \rightarrow {}^4T_1$ and $^4A_2 \rightarrow {}^4T_2$ transitions of Cr^{3+} ions, respectively.

As shown in Figure 2b, the PL spectrum of the $AlPO_4$:0.3%Cr^{3+} phosphor exhibits several peaks centering at 684, 694, 701 and 707 nm; in which, the narrow-deep emission peaking at 694 nm shows the highest intensity. It was reported that there were several levels of low energy in the incompleted $3d^3$ electronic shell of Cr^{3+} ions and luminescent emissions could be generated by optical transitions [23].

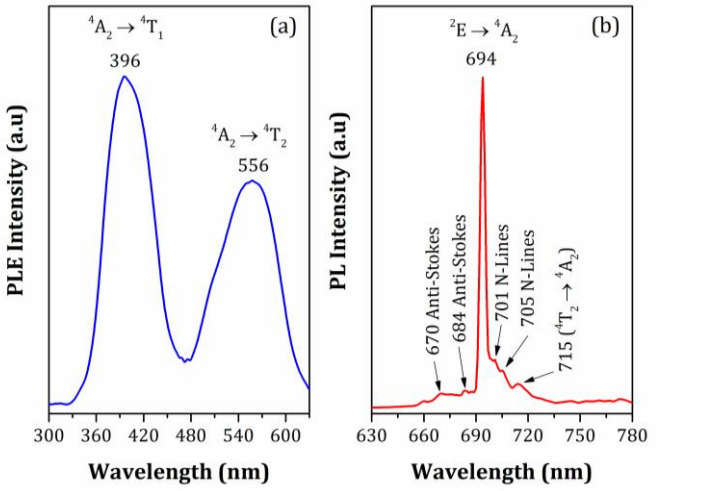

Figure 2. (a) PLE spectrum measured for the 694 nm emission; (b) PL spectra of the $AlPO_4$:0.3%Cr^{3+} phosphor annealed at 1500 °C for 5h in air, measured under the excitation wavelength of 394 nm.

Figure 3 illustrates the levels of Cr^{3+} ions in an octahedral crystal field presented in the Tanabe–Sugano diagram; in which, ^4F level can split into the $^4A_2$, $^4T_2$ and $^4T_1$, while the ^2G level can split into the ^2E, $^2T_1$, $^2T_2$ and $^2A_1$ [24]. The $^4A_2$ which is considered as the ground state has the lowest energy [23, 24]. Tanabe–Sugano diagram in Figure 3 describes the relationship between energy splitting levels (E/B) and the crystal field strength (D_q/B) where D_q is the octahedral crystal ligand field splitting parameter and B is the Racah parameter [25].

The energy level of excited state ^2E shows a similar value with that of $^2T_1$ state for different field strengths; hence, there is only a narrow-band emission generated by the $^2E \rightarrow {}^4A_2$ transition.On the contrary , the other energy levels of $^4T_2$, $^4T_1$, $^2A_1$ states are more influenced by the field strength, inducing a broad emission band [26, 27].Specifically , Cr^{3+} ions could stay in weak, medium or strong crystal-field site where the Dq/B value is less, equal or higher than 2.3, respectively. For a weak crystal field, an obvious broadband in the PL could be related to the improvement of the phonon assisted $^4T_2 \rightarrow {}^4A_2$ transitions, explained by the higher level of the excited ^2E state in comparison with $^4T_2$ state. For a medium crystal field, there will be a superpostion between $^4T_2$ and ^2E state. Then, the PL spectrum shows a coincidence of the broadband emission resulted by $^4T_2 \rightarrow {}^4A_2$ transition and R lines generated by the $^2E \rightarrow {}^4A_2$ transition and phonon sideband transitions. For a strong crystal-field site, the excited ^2E state has the lowest energy level and there are narrow zero-phonon lines (R lines) in the PL spectrum [9, 14]. According to Huyen et al., the lattice parameters D_q, B and D_q/B could be derived from the excitation spectrum, giving that D_q = 1798.6 cm^{-1}, B = 729 cm^{-1} and D_q/B = 2.47 [6, 11, 13]. These results reveal that the surrounding site of Cr^{3+} ions has a strong crystal field. As shown in Figure 2b, the PL spectrum illustrates a narrow emission band with the FWHM of only ~4 nm peaking at 694 nm, possibly contributing to the $^2E \rightarrow {}^4A_2$ transition of Cr^{3+} ions [4, 9]. In addition, the band peaking at 670 nm and 684 nm can be assigned to the contribution of anti-Stokes of Cr^{3+} emission [28]. While 707-nm sharpened N-line could be related to the enhancement in the number of Cr^{3+} ion-coupling states (N line)

or to the vibronic transitions [29], the 715-nm emission peak is ascribed to the $^4T_2 \rightarrow {}^4A_2$ transition [4, 5, 15].

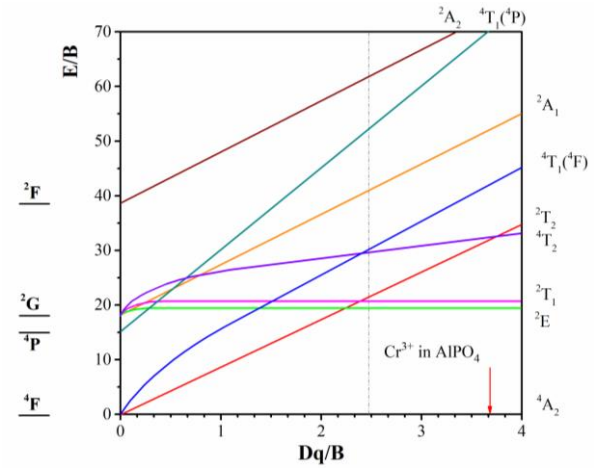

Figure 3. Tanabe–Sugano diagram of Cr^{3+} ions in the octahedral crystal field (a); energy levels of the Cr^{3+} ions in a weak crystal field (b); a medium crystal field (c) and a strong crystal field (d).

In order to investigate the influence of annealing temperature on the optical properties, the PL spectra of the $AlPO_4$:0.3%Cr^{3+} powder prepared at a variety of temperatures have been recorded and represented in Figure 4. It is worth noticing that the PL intensity of the 694 nm is continuously increased in the temperature range of 1200 - 1500 °C. Additionally, the enhancement in the 694-nm peak intensity may be contributed by the better diffusion process of Cr^{3+} ions with a higher annealing temperature [30].

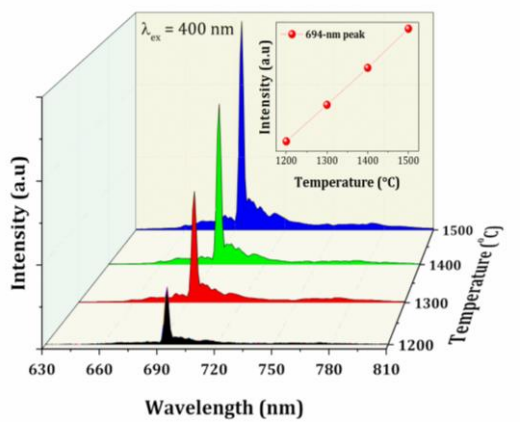

Figure 4. Tanabe–Sugano diagram of Cr^{3+} ions in the octahedral crystal field (a); energy levels of the Cr^{3+} ions in a weak crystal field (b); a medium crystal field (c) and a strong crystal field (d).

The PL spectra of the $AlPO_4$:x%Cr^{3+} (x = 0.1−1.5%) phosphors air-annealed at 1500 °C for 5 h have been carried out and the results excited by the two different wavelengths of 400 nm and 560 nm are shown in Figures 5a&b. Although the PL patterns of all $AlPO_4$:x%Cr^{3+} phosphors share a similar shape, the PL intensity is significantly influenced by the Cr^{3+} doping level. The insets of Figures 5a&b show that the PL intensity achieves the highest value at the doping level of 0.3%, then decreases with a higher

concentration of Cr^{3+} ions. It is reported that the distance of adjacent Cr^{3+} ions is too large with the low concentration of Cr^{3+} ions, leading to the low luminescent intensity due to the low density of luminescent centers [6]. With a higher level of Cr^{3+} ions, the distance between two neighbour Cr^{3+} ions becomes shorter, making the easier transfer of energy among Cr^{3+} ions. After reaching a threshold value when the distance reaches the critical distance, the PL intensity decreases, as shown in Figures 5a&b. It could be explained by the quenching phenomenon by concentration [31–33].

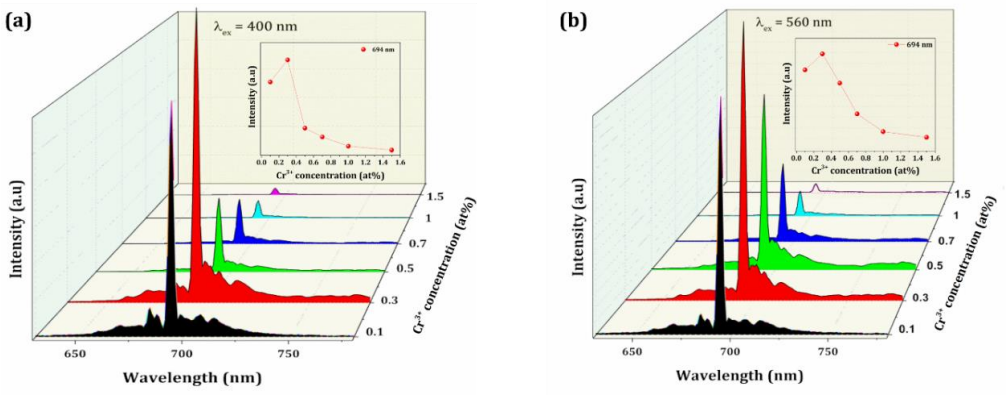

Figure 5. 3D PL spectra of $AlPO_4$: x%Cr^{3+} (x = 0.1-1.5%) phosphors air-annealed at 1500 °C for 5h under the excitation wavelength of (a) 400 nm and (b) 560 nm.

To further study how the luminescent quenching phenomenon occurs, the critical distance (R_c) has been calculated by following the Blasse equation [31, 34, 35]:

$$R_c \approx 2R = 2\left(\frac{3V}{4\pi X_c N}\right)^{\frac{1}{3}} \qquad (1)$$

In which, V is volume of the unit cell, X_c is the threshold of the Cr^{3+} ions concentration when the PL intensity starts decreasing and N is the number of the unit cells. For the annealed-at-1500 °C sample, with V= 352 $Å^3$, X_c= 0.3 mol%, N= 2, the calculated R_c value is 32.74 Å, which is quite close to the previous R_c reported for Cr^{3+}-doped phosphor [6, 31, 34, 36, 37]. This R_c value is much greater than the critical distance of 5 Å for an effective interaction of energy transfer mechanism, implying that the multipolar interaction is accounted for the phosphorus quenching [31, 34, 36, 37]**.** In addition, there are three main types of the multipolar interactions: dipole-dipole, dipole-quadrupole, quadrupole-quadrupole interactions [34, 37]. According to Dexter theory [10, 13, 14, 38, 39], the correlation between the emission intensity and the quenching Cr^{3+} ions level could be this reduced equation [34]:

$$\log\left(\frac{I}{X}\right) = C - \frac{\theta}{3}\log(X) \qquad (2)$$

Where C is a constant and X is the Cr^{3+} concentration when the quenching phenomenon occurs. θ is the corresponding function to each multipolar interaction, taking the value of 6, 8, 10 which are corresponding to the dipole-dipole, dipole-quadrupole, quadrupole-quadrupole interactions [34, 37].

The relationship between log(I/X) and log(X) using the different excitation wavelength is shown in Figure 6. Here, θ could be determined as a linear coefficient, giving the estimated values of 0.948 and 0.951 for the excitation wavelength of 400 nm and 560 nm. These values are more close to 6 than 8 or

10. Thus, it is predicted that the dipole-dipole interaction is the significant factor in the multipolar interaction of Cr^{3+} ions [34].

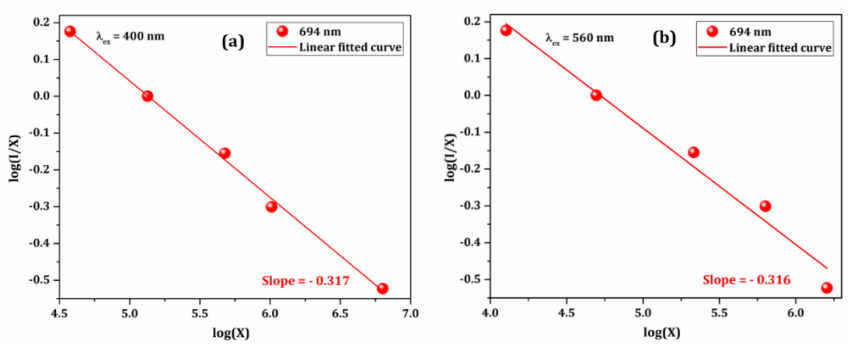

Figure 6. The relationship between log (I/x) and log (x) excited by the wavelength of (a) 400 nm and (b) 560 nm.

The color coordinates (x, y) of PL spectra for the samples doped with various Cr^{3+} ions levels are shown in Table 2. Because the PL spectra show a resemble pattern, the (x, y) coordinates are quite similar with the various concentrations of Cr^{3+} ions.

Table 2. The (x, y) coordinates of PL spectra for the samples doped with numerous Cr^{3+} ions levels.

%Cr^{3+}	(x, y)
0.1	(0.7105, 0.2894)
0.3	(0.7121, 0.2878)
0.5	(0.6971, 0.3027)
0.7	(0.6911, 0.3088)
1.0	(0.6709, 0.3289)
1.5	(0.6562, 0.3435)

Hence, only the chromatic coordinate of the optimized sample ($AlPO_4$:0.3%Cr^{3+}) is illustrated at x = 0.7121; y = 0.2878 on CIE Chromaticity diagram in Figure 7. It is noted that this coordinate is quite adjacent to some far-red phosphors such as $KLaMgWO_6$:0.6%Mn^{4+} (0.7205, 0.2794) [40], $ZnGa_2O_4$:Cr^{3+} (0.678, 0.263) [41] which were previously reported. Hence, the $AlPO_4$:Cr^{3+} phosphor could be useful as a deep far-red luminescence material for WLED applications.

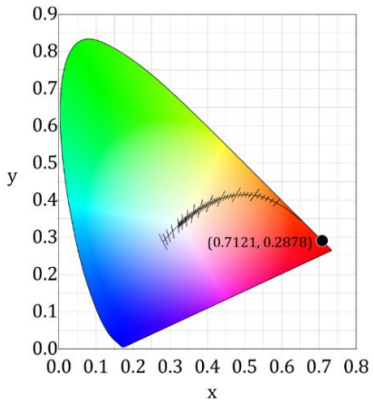

Figure 7. CIE chromaticity coordinate of $AlPO_4$:0.3%Cr^{3+} sample annealed at 1500 °C for 5h in air.

To make a proof of concept, a purple LED prototype was prepared by coating the $AlPO_4$:0.3%Cr^{3+} powder on a 395-nm (UV) LED chip. The electroluminescence (EL) spectra of uncoated- and coated-phosphor UV chips are illustrated in Figure 8a, in which, the inset shows the EL spectrum of phosphor-coated chip. The inset in Figure 8a exhibits two intensively sharp emissions peaking at 395 nm and 694 nm, corresponding to participation of the UV LED chip and the $AlPO_4$:0.3%Cr^{3+} powder. As shown in Figure 8b, the color coordinates of the LED are (x=0.2412; y=0.1330), showing a shift towards the blue region in comparison with $AlPO_4$:0.3%Cr^{3+} phosphor. The digital image of the LED prototype is given in the inset of Figure 8b with OFF and ON mode, demonstrating that the purple LED prototype was successfully fabricated.

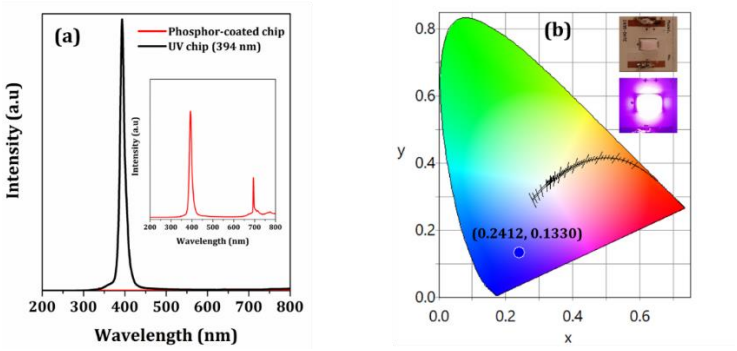

Figure 8. (a) The comparison between the electroluminescence spectrum of bared UV chip and phosphor-coated chip (the inset shows the zoom-out EL spectrum of phosphor-coated chip) and (b) CIE chromaticity diagram of a prototype purple LED fabricated by coating the $AlPO_4$:0.3%Cr^{3+} phosphor on a 410-nm (UV) LED chip.

4. Conclusion

In this paper , $AlPO_4$:Cr^{3+} powder with extremely sharp emission band (FWHM~4 nm) peaking at 694 nm was synthesized by a facile sol-gel method. The Tanabe–Sugano diagram demonstrates that the neigbour sites surrounding Cr^{3+} ions is a strong crystal field (D_q/B=2.47) and the 694-nm peak could be attributed to the $^2E \rightarrow {}^4A_2$ transition of Cr^{3+} ions. The highest PL intensity was achieved for the $AlPO_4$:0.3%Cr^{3+} sample. By coating the $AlPO_4$:0.3%Cr^{3+} phosphor on a UV LED chip, a prototype of purple LED was effectively made, giving the color coordinates (x, y) of (0.2412, 0.1330). Therefore, it is promising to use $AlPO_4$:Cr^{3+} powder as an interesting deep-red phosphor for the horticulture lighting.

Acknowledgments

This research was funded by PHENIKAA University under Grant 01.2019.03.

References

[1] Y. Ren, R. Cao, T. Chen, L. Su, X. Cheng, T. Chen, S. Guo, X. Yu, Photoluminescence Properties of Ba_2LaSbO_6:Mn^{4+} Deep-red-emitting Phosphor for Plant Growth LEDs, J. Lumin., Vol. 209, 2019, pp. 1–7. https://doi.org/10.1016/j.jlumin.2019.01.014.

[2] D. Q. Trung, N. Tu, N. V. Quang, M. T. Tran, N. V. Du, P. T. Huy, Non-rare-earth Dual Green and Red-emitting Mn-doped $ZnAl_2O_4$ Phosphors for Potential Application in Plan-growth LEDs, J. Alloys Compd., Vol. 845, 2020, pp. 2–10. https://doi.org/10.1016/j.jallcom.2020.156326.

[3] Y. Xu, Y. Zhang, L. Wang, M. Shi, L. Liu, Y. Chen, Red Emission Enhancement for $CaAl_{12}O_{19}:Cr^{3+}$ and $CaAl_{12}O^{19}:Mn^{4+}$ phosphors, J. Mater. Sci. Mater. Electron., Vol. 28, 2017, pp. 12032–12038. https://doi.org/10.1007/s10854-017-7014-3.

[4] K. Li, H. Lian, R. Van Deun, A Novel Deep Red-emitting Phosphor $KMgLaTeO_6:Mn^{4+}$ with High Thermal Stability and Quantum Yield for W-LEDs: Structure, Site Occupancy and Photoluminescence Properties, Dalt. Trans., Vol. 47, 2018, pp. 2501–2505. https://doi.org/10.1039/c7dt04811d.

[5] Q. Sun, S. Wang, B. Devakumar, L. Sun, J. Liang, X. Huang, Synthesis, Crystal Structure, and Photoluminescence Characteristics of High-Efficiency Deep-Red Emitting $Ba_2GdTaO_6:Mn^{4+}$ Phosphors, ACS Omega., Vol. 4, 2019, pp. 13474–13480. https://doi.org/10.1021/acsomega.9b01787.

[6] N. T. Huyen, N. Tu, D. T. Tung, D. Q. Trung, D. D. Anh, T. T. Duc, T. T. T. Nga, T. Huy, Photoluminescent Properties of Red-emitting Phosphor $BaMgAl_{10}O^{17}:Cr^{3+}$ for Plant Growth LEDs, Opt. Mater. J., Vol. 108, 2020. https://doi.org/10.1016/j.optmat.2020.110207.

[7] J. Liang, L. Sun, B. Devakumar, S. Wang, Q. Sun, H. Guo, B. Li, X. Huang, Novel Mn^{4+}-activated $LiLaMgWO_6$ Far-red-emitting Phosphors: High Photoluminescence Efficiency, Good Thermal Stability, and Potential Applications in Plant Cultivation LEDs, RSC Adv., Vol. 8, 2018, pp. 27144–27151. https://doi.org/10.1039/c8ra05669b.

[8] J. Chen, C. Guo, Z. Yang, T. Li, J. Zhao, $Li_2SrSiO_4:Ce^{3+}$, Pr^{3+} Phosphor with Blue, Red, and Near-Infrared Emissions Used for Plant Growth LED, J. Am. Ceram. Soc., Vol. 99, 2016, pp. 218–225. https://doi.org/10.1111/jace.13952.

[9] C. R. Ronda, T. Jüstel, H. Nikol, Rare Earth Phosphors: Fundamentals and Applications, J. Alloys Compd., Vol. 275–277, 1998, pp. 669–676. https://doi.org/10.1016/S0925-8388(98)00416-2.

[10] F. B. Xiong, H. Chen, H. F. Lin, X. G. Meng, E. Ma, W.Z. Zhu, Photoluminescence Characteristics of Sm^{3+}-doped $LnBWO_6$ (Ln = La, Gd and Y) as New Orange-red Phosphors, J. Lumin., Vol. 209, 2019, pp. 89–94. https://doi.org/10.1016/j.jlumin.2019.01.034.

[11] H. S. Jang, W. B. Im, D. C. Lee, D. Y. Jeon, S. S. Kim, Enhancement of Red Spectral Emission Intensity of $Y_3Al_5O_{12}:Ce^{3+}$ Phosphor via Pr Co-doping and Tb Substitution for the Application to White LEDs, J. Lumin., Vol. 126, 2007, pp. 371–377. https://doi.org/10.1016/j.jlumin.2006.08.093.

[12] S. B. Aldabergenova, A. Osvet, G. Frank, H. P. Strunk, P. C. Taylor, A. A. Andreev, Blue, Green and Red Emission from Ce^{3+}, Tb^{3+} and Eu^{3+} Ions in Amorphous GaN and AlN Thin Films, J. Non. Cryst. Solids., Vol. 299–302, 2002, pp. 709–713. https://doi.org/10.1016/S0022-3093(01)01211-X.

[13] L. Wu, B. Liu, J. Zhang, B. Han, A Novel UV-emitting Ce^{3+}-doped Chloroborate $Ba_2GaB_4O_9Cl$ Phosphor, Optik (Stuttg)., Vol. 184, 2019, pp. 241–246. https://doi.org/10.1016/j.ijleo.2019.03.064.

[14] J. Zhang, Y. Dai, P. Huang, J. Yu, L. Zhao, B. Han, Orange Emission of Sm^{3+} in a Double Phosphate $KMgLa(PO4)_2$ under Near-ultraviolet Excitation, Optik (Stuttg)., Vol. 153, 2018, pp. 81–85. https://doi.org/10.1016/j.ijleo.2017.09.128.

[15] A. Xie, X. Yuan, F. Wang, Y. Shi, Z. Mu, Enhanced Red Emission in $ZnMoO_4:Eu^{3+}$ by Charge Compensation, J. Phys. D. Appl. Phys. 43 (2010) 055101. https://doi.org/10.1088/0022-3727/43/5/055101.

[16] A. Kostyukov, M. Baronskiy, A. Rastorguev, V. Snytnikov, V. Snytnikov, A. Zhuzhgov, A. Ishchenko, Photoluminescence of Cr^{3+} in Nanostructured Al_2O_3 Synthesized by Evaporation Using a Continuous Wave CO_2 Laser, RSC Adv., Vol. 6, 2016, pp. 2072–2078. https://doi.org/10.1039/c5ra19455e.

[17] A. Xie, X. Yuan, F. Wang, Y. Shi, Z. Mu, Enhanced Red Emission in $ZnMoO_4$: Eu^{3+} by Charge Compensation, J. Phys. D. Appl. Phys., Vol. 43, 2010, pp. 055101. https://doi.org/10.1088/0022-3727/43/5/055101.

[18] K. Ogasawara, F. Alluqmani, H. Nagoshi, Multiplet Energy Level Diagrams for Cr^{3+} and Mn^{4+} in Oxides with O_h Site Symmetry Based on First-Principles Calculations, ECS J. Solid State Sci. Technol. 5 (2016) R3191–R3196. https://doi.org/10.1149/2.0231601jss.

[19] Q. Sai, C. Xia, H. Rao, X. Xu, G. Zhou, P. Xu, Mn,Cr-co-doped $MgAl_2O_4$ Phosphors for White LEDs, J. Lumin. Vol. 131, 2011, pp. 2359–2364. https://doi.org/10.1016/j.jlumin.2011.05.046.

[20] T. Phan, M. Phan, S. Yu, A new band in Cr^{3+}-doped $MgAl_2O_4$ Natural Spinel, Physica Status Solidi (b), Vol. 241, No. 2, 2014, pp.434-438. https://doi.org/10.1002/pssb.200301918.

[21] Y. F. Liu, Z. P. Yang, Q. M. Yu, Preparation and Its Luminescent Properties of $AlPO_4:Eu^{3+}$ Phosphor for W-LED Applications, J. Alloys Compd., Vol. 509, 2011, pp. L199–L202. https://doi.org/10.1016/j.jallcom.2011.03.064.

[22] M. T. Tran, N. Tu, N. V Quang, N. D. Hung, L. T. H. Thu, D. Q. Trung, P.T. Huy, Excellent Thermal Stability and High Quantum Efficiency Orange-red-emitting $AlPO_4:Eu^{3+}$ Phosphors for WLED Application, J. Alloys Compd., 2020, pp. 156941. https://doi.org/https://doi.org/10.1016/j.jallcom.2020.156941.

[23] V. Singh, R. P. S. Chakradhar, J. L. Rao, K. Al-Shamery, M. Haase, Y.-D. Jho, Electron Paramagnetic Resonance and Photoluminescence Properties of α-$Al_2O_3:Cr^{3+}$ Phosphors, Appl. Phys. B Lasers Opt., Vol. 107, 2012, pp. 489–495. https://doi.org/10.1007/s00340-012-4993-x.

[24] Y. Tanabe, S. Sugano, On the Absorption Spectra of Complex Ions. Parts I and II, J. Phys. Soc. Japan., Vol. 9, No. 753–766, 1954, pp. 766–779. https://doi.org/10.1143/JPSJ.9.753.

[25] C. Wang, A. Wadhwa, S. Cui, R. Ma, X. Qiao, X. Fan, X. Zhang, Dual Mode Temperature Sensing through Luminescence Lifetimes of F- and O-coordinated Cr^{3+} Sites in Fluorosilicate Glass-ceramics, RSC Adv., Vol. 7, 2017, pp. 52435–52441. https://doi.org/10.1039/c7ra10864h.

[26] A. Mondal, J. Manam, Investigations on Spectroscopic Properties and Temperature Dependent Photoluminescence of Cr^{3+}-doped $MgGa_2O_4$ Phosphor, Mater. Res. Express., Vol. 6, 2019, pp. 095081. https://doi.org/10.1088/2053-1591/ab317e.

[27] M. G. Brik, N. M. Avram, C. N. Avram, Comparative Crystal Field Calculations of the Cr^{3+} Energy Level Schemes in $ZnAl_2S_4$ and $ZnGa_2O_4$, J. Mater. Sci. Mater. Electron., Vol. 20, 2009, pp.30–32. https://doi.org/10.1007/s10854-007-9426-y.

[28] L. Marciniak, A. Bednarkiewicz, J. Drabik, K. Trejgis, W. Strek, Optimization of Highly Sensitive YAG:Cr^{3+},Nd^{3+} Nanocrystal-based Luminescent Thermometer Operating in an Optical Window of Biological Tissues, Phys. Chem. Chem. Phys., Vol. 19, 2017, pp. 7343–7351. https://doi.org/10.1039/c6cp07213e.

[29] G. Rani, P.D. Sahare, Structural and Photoluminescent Properties of $Al_2O_3:Cr^{3+}$ Nanoparticles via Solution Combustion Synthesis Method, Adv. Powder Technol., Vol. 25, 2014, pp. 767–772. https://doi.org/10.1016/j.apt.2013.11.009.

[30] J. Park, G. Kim, Y.J. Kim, Luminescent Properties of $CaAl_4O_7$ Powders Doped with Mn^{4+} Ions, Ceram. Int., Vol. 39, 2013, pp. S623–S626. https://doi.org/10.1016/j.ceramint.2012.10.149.

[31] J. Liu, J. Ma, Z. Wu, J. Sun, Z. Li, Study on Synthesis, Optimization and Concentration Quenching Mechanism of Deep-blue-emitting $BaNa(B_3O_5)_3:Eu^{2+}$ Phosphor, Optik (Stuttg)., Vol. 154, 2018, pp. 421–427. https://doi.org/10.1016/j.ijleo.2017.10.103.

[32] T. T. H. Tam, N. V Du, N. D. T. Kien, C. X. Thang, N. D. Cuong, P. T. Huy, N. D. Chien, D. H. Nguyen, Co-Precipitation Synthesis and Optical properties of Green-emitting $Ba_2MgSi_2O_7:Eu^{2+}$ Phosphor, Journal of Luminescence, 147, 2014, pp. 358–362. https://doi.org/10.1016/j.jlumin.2013.11.066.

[33] L. T. T. Vien, N. Tu, M. T. Tran, N. V. Du, D. H. Nguyen, D. X. Viet, N. V. Quang, D. Q. Trung, P. T. Huy, A New Far-red Emission from Zn_2SnO_4 Powder Synthesized by Modified Solid State Reaction Method, Opt. Mater. (Amst), Vol. 100, 2020, p.109670. https://doi.org/10.1016/j.optmat.2020.109670.

[34] M. K. Hussen, F. B. Dejene, Effect of Cr^{3+} Doping on Structural and Optical Property of $ZnGa_2O_4$ Synthesized by Sol-gel Method, Opt. - Int. J. Light Electron Opt., Vol. 181, 2019, pp. 514–523. https://doi.org/10.1016/j.ijleo.2018.12.121.

[35] G. Blasse, Energy Transfer Between Inequivalent Eu^{2+} Ions, J. Solid State Chem., Vol. 62, 1986, pp. 207–211. https://doi.org/10.1016/0022-4596(86)90233-1.

[36] L. T. T. Vien, N. Tu, T. T. Phuong, N. T. Tuan, N. V. Quang, H. V. Bui, A. T. Duong, D. Q. Trung, P. T. Huy, Facile Synthesis of Single Phase α-$Zn_2SiO_4:Mn^{2+}$ Phosphor via High-energy Planetary Ball Milling and Post-annealing Method, J. Lumin., Vol. 215, 2019, pp. 116612. https://doi.org/10.1016/j.jlumin.2019.116612.

[37] S. V. Motloung, F. B. Dejene, H. C. Swart, O. M. Ntwaeaborwa, Effects of Cr^{3+} Mol% on the Structure and Optical Properties of the $ZnAl_2O_4:Cr^{3+}$ Nanocrystals Synthesized Using Sol-gel Process, Ceram. Int., Vol. 41, 2015, pp. 6776–6783. https://doi.org/10.1016/j.ceramint.2015.01.124.

[38] J. Li, H. Yan, F. Yan, A Novel Orange-red-emitting Borate-based Phosphor for NUV Pumped LEDs, Optik (Stuttg)., Vol. 127, 2016, pp. 5984–5989. https://doi.org/10.1016/j.ijleo.2016.04.022.

[39] B. Han, B. Liu, J. Zhang, Y. Dai, $K_3YB_6O_{12}:Sm^{3+}$: A Novel Orange-red Emitting Phosphor for White Light-emitting Diodes, Optik (Stuttg)., Vol. 179, 2019, pp. 346–350. https://doi.org/10.1016/j.ijleo.2018.10.221.

[40] J. Liang, B. Devakumar, L. Sun, Q. Sun, S. Wang, B. Li, D. Chen, X. Huang, Mn^{4+}-activated $KLaMgWO_6$: A New High-efficiency Far-red Phosphor for Indoor Plant Growth LEDs, Ceram. Int. 45 (2019) 4564–4569. https://doi.org/10.1016/j.ceramint.2018.11.143.

[41] M. Li, H. Zhang, X. Zhang, J. Deng, Y. Liu, Z. Xia, B. Lei, Cr^{3+}-doped $ZnGa_2O_4$ Far-red Emission Phosphor-in-glass: Toward High-power and Color-stable Plant Growth LEDs with Responds to All of Phytochrome, Mater. Res. Bull. 108 (2018) 226–233. https://doi.org/10.1016/j.materresbull.2018.09.014.